Khayrudinov, Vladislav; Koskinen, Tomi; Grodecki, Kacper; Murawski, Krzysztof; Kopytko, Małgorzata; Yao, Lide; Jiang, Hua; Tittonen, Ilkka Juhani; Lipsanen, Harri; Haggren, Tuomas

InSb Nanowire Direct Growth on Plastic for Monolithic Flexible Device Fabrication

Published in:
ACS Applied Electronic Materials

DOI:
10.1021/acsaelm.1c01175

Published: 25/01/2022

Document Version
Publisher's PDF, also known as Version of record

ACS APPLIED ELECTRONIC MATERIALS

pubs.acs.org/acsaelm

Article

InSb Nanowire Direct Growth on Plastic for Monolithic Flexible Device Fabrication

Vladislav Khayrudinov,* Tomi Koskinen, Kacper Grodecki, Krzysztof Murawski, Małgorzata Kopytko, Lide Yao, Hua Jiang, Ilkka Juhani Tittonen, Harri Lipsanen, and Tuomas Haggren

Cite This: *ACS Appl. Electron. Mater.* 2022, 4, 539−545

Read Online

ACCESS | Metrics & More | Article Recommendations

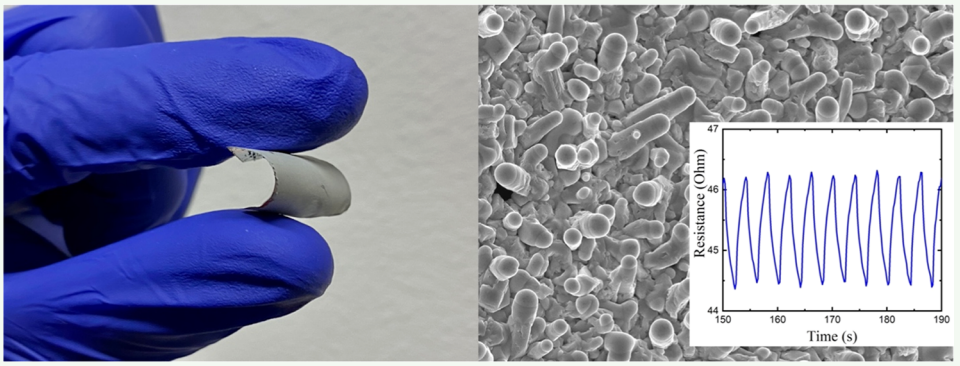

ABSTRACT: We report direct growth of InSb nanowires (NWs) and monolithic device fabrication on flexible plastic substrates. The nanowires were grown using metal−organic vapor-phase epitaxy (MOVPE) in self-catalyzed mode. The InSb NWs are shown to form in the zinc-blende crystal structure and to exhibit strong photoluminescence at room temperature. The NW array light-trapping properties are evidenced by reflectance that is significantly reduced compared to bulk material. Finally, the InSb NWs are used to demonstrate a metal−semiconductor−metal photoresistor directly on the flexible plastic substrate. The results are believed to advance the integration of III−V nanowires to flexible devices, and infrared photodetectors in particular.

KEYWORDS: *InSb nanowires, flexible, bendable, photoluminescence, MOVPE/MOCVD, photoresistor*

INTRODUCTION

III−V semiconductor nanowires (NWs) have been extensively studied over the last 2 decades, propelling the research of numerous intriguing nanowire-based functional devices such as lasers,[1−3] light-emitting diodes (LEDs),[4] all-optical logic components,[5] solar cells,[6] and photodetectors.[7] At the same time, the development of flexible and wearable electronics has been progressing at an unprecedented pace, resulting in a vast range of applications, from flexible photodetectors[8] and photonic circuits[9] to bendable batteries,[10] soft solar cells,[11] and so on.[12] III−V semiconductors are particularly promising for flexible optoelectronic devices due to their extraordinary properties such as tunable direct band gap, efficient light scattering[13] and trapping,[6] excellent strain relaxation, and high carrier mobility.[14] InSb is one interesting example of III−V semiconductors that has a narrow direct band gap, strong spin−orbit coupling, and high mobility. It has been particularly useful in quantum and infrared wavelength range optoelectronics applications including infrared photodetectors,[15] field-effect transistors,[16] Majorana fermions detectors,[17] and others.[18] However, there is a lack of reports on light-emitting InSb NWs and the reports on photoluminescence measurements of InSb NWs are literally nonexistent.

As noted above, flexible devices have attained significant interest recently due to their applicability to a much broader range of end uses. Direct growth on flexible plastics is the most straightforward pathway for flexible devices; however, growth on plastics has always been very challenging (especially using metal−organic vapor-phase epitaxy (MOVPE) and molecular beam epitaxy (MBE)) due to temperature limitations and a noncrystalline polymer surface. As a result, the typical approach to attain NWs in plastic relies on the growth of NWs on a crystalline substrate and on a subsequent complex multistep transfer process,[19−21] after which the crystalline substrate can be polished for subsequent NW growth.[22] As an

Received: November 23, 2021
Accepted: January 4, 2022
Published: January 11, 2022

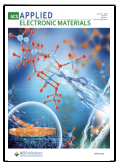

alternative, we have previously shown that it is in fact feasible and significantly more straightforward to grow III−V NWs directly on polyimide,[23] in particular when using low-temperature growth regime.[24] Presently, literature reports include InSb NW growth on crystalline substrates,[25−30] as well as InP and InAs NWs on polyimide.[23] However, no previous report has demonstrated any type of crystalline InSb growth on plastic substrates with the exception of electrochemical deposition on polycarbonate membranes.[31] It should be emphasized here that heteroepitaxial growth, especially in the case of NWs, is not straightforward[14,32] and the possibility of InSb growth on plastic cannot be deduced based on the growth of other III−V materials on plastic or on InSb NW growth on crystalline substrates. On the other hand, InSb has several unique properties among III−V semiconductors that enable its use for applications where other III−V materials are not applicable. Perhaps most importantly, the narrow band gap of ∼170 meV is the lowest among binary III−V materials and allows the detection or emission of wavelengths up to ∼8 μm. This wavelength range is critical for numerous applications, such as those where visibility through smoke or fog is required highlighting the importance of InSb as a material.

In this work, we demonstrate InSb NW growth directly on flexible plastic substrates with a crystal quality that enables photoluminescence even at room temperature. The InSb NWs were grown using metal−organic vapor-phase epitaxy (MOVPE) system on polyimide (PI) substrates directly inside the growth reactor from in situ deposited In droplets. The NWs are found to be crystalline in the zinc-blende phase. We show that InSb NWs are optically active and emit photoluminescence signals even at room temperature. In addition, the NW forest exhibits low reflectance in mid- and long-wave infrared regions. To the best of our knowledge, this is the first demonstration of photoluminescence emission from InSb NWs in general and the first report of InSb NWs on plastic substrates. Finally, the InSb NWs on flexible plastic are used to demonstrate a monolithic photoresistor. The photoresistor fabrication process required just two processing steps: (1) InSb growth on plastic without any substrate preparation steps and (2) metal contact deposition. We believe that the results will advance the integration of InSb NWs to flexible optoelectronics by providing straightforward means for direct fabrication on plastics.

EXPERIMENTAL SECTION

InSb NWs were synthesized on flexible plastic substrates directly inside a horizontal-flow atmospheric-pressure metal−organic vapor-phase epitaxy (MOVPE). Flexible nonconductive 25 μm thick polyimide tape (Polyonics, XT-621) was used as a growth substrate. Trimethylindium (TMIn), tertiary butylarsine (TBAs), and trimethylantimony (TMSb) were used as precursors. Prior to the growth, the MOVPE reactor was heated to 440 °C under a hydrogen atmosphere. The growth of the InSb NWs and network was performed in three steps in the MOVPE reactor: first, In seed particles were deposited for 15 s, followed by a short (300 s) InAs segment growth followed by a significantly longer (3600 s) InSb crystal growth. It should be emphasized that the growth requires no pre-processing such as seed layer deposition before loading to the MOVPE reactor, and the In seed particle deposition or InAs stub growth incur no additional complexity to the fabrication as the growth takes place fully inside the MOVPE reactor in a single growth run (including In seed particles, InAs initial segment, and InSb growth). In more detail, the In particles were deposited in situ using a TMIn flow of 5.95 μmol/min. Next, InAs stubs were grown in situ with the nominal V/III ratio of 2 by introducing TBAs (12.6 μmol/min) into the reactor while keeping the TMIn flow open. Directly afterward, InSb NW growth with a nominal V/III ratio of 2 was initiated by closing TBAs flow and opening the TMSb flow (12.46 μmol/min) while keeping the TMIn flow open. After the growth, the samples were cooled down under TMSb flow. Hydrogen was used as a carrier gas, and the total reactor gas flow rate was ∼5 L/min (slm). The growth temperatures reported in this work are thermocouple readings of the lamp-heated graphite susceptor, which are slightly (approximately tens of °C) higher than the real substrate surface temperature. The structural properties and morphology of the NWs were studied using scanning electron microscopy (SEM) (Zeiss Supra 40) operated at 5−15 keV. High-resolution transmission electron microscopy (TEM) measurements were carried out with a JEOL 2200FS double-aberration-corrected FEG microscope operated at 200 kV. The elemental composition of the NWs was determined using a TEM-integrated energy-dispersive X-ray spectroscopy (EDX) tool. Crystal orientation was determined from electron diffraction pattern according to $1/d^2 = (k^2 + k^2 + l^2)/a^2$, where d is the observed distance in the diffraction pattern; h, k, and l are Miller indices; and a = 0.648 nm is the InSb lattice constant. It was also verified that the obtained crystal planes have the expected angles between them. The TEM lamella of a nanowire was prepared by focused ion beam (FIB) milling using Ga^+ ions accelerated at 30 kV in a JEOL JIB-4700F multibeam system. To reduce charging and ion-beam damage during FIB processing, we predeposited a 12 nm thick carbon layer on the as-grown NWs using a sputtering system (Leica EM ACE600) before loading the sample into the FIB chamber. Next, a 1.0 μm thick carbon layer with dimension 5 × 1 μm^2 was grown to cover a target NW using ion-beam-induced deposition inside the FIB. After cutting off, the NW covered by carbon layer was processed as a lamella and was lifted out of the substrate using an OmniProbe manipulator and transferred onto a TEM grid. Finally, the cross-sectional lamella was fine-polished to about 50 nm in thickness by Ga^+-ion milling. Photoluminescence measurements were performed using a Vertex v70 Fourier transform infrared (FTIR) spectrometer. The optical path was completely under vacuum conditions. During the measurements, the samples were placed in a closed-cycle helium cryostat, which allows precise control of the temperature from 20 to 300 K. The cryostat was equipped with ZnSe optical windows that allow the measurements in the range up to 19 μm. PL was measured in step-scan mode with an MCT photodetector and a lock-in amplifier. As an excitation source, a 637 nm line laser chopped mechanically with a frequency of 1000 Hz was used. The reflectance was measured with a Bruker Vertex v70 IR spectrometer. A Globar was used as a measurement source, and an MCT D313 photodetector cooled with liquid nitrogen was used as a detection element. The optical paths were under vacuum, and the reflectance measurements were performed in Rapid Scan mode using a 4 mm transmission gap. Current−voltage characteristics in the dark and under illumination as well as photoresponse of electrical resistance as a function of time were measured using a source meter (Keithley 2602B). Prior to measurement, gold-coated probes were carefully brought in contact with Ti/Au contact pads evaporated on the ends of the sample through a shadow mask. Electron beam evaporation (Edwards E306A) was used to deposit Ti/Au (20/100 nm) rectangle contact pads (4 mm × 7 mm) at the ends of the sample with the separation of 6 mm in between. Overall, the final device was fabricated monolithically on a flexible substrate in only two steps: InSb NW growth in MOVPE, followed by Ti/Au contact pads evaporation through a shadow mask. The two-step device structure schematic is depicted in Figure 5a. The $I-V$ curve was measured with a solar simulator (Asahi Spectra HAL-320) illuminating the sample under well-defined AM1.5 equivalent conditions. The photoresponsivity of resistance was studied by chopping the light source on and off at an interval of 2 s and recording the corresponding $I-V$ characteristics. The resistance at each time step was obtained from linear fits to IV curves (seven points between −1 and 1 mA). Prior to the bending measurements, similar Ti/Au contact pads were deposited at the ends of the 8 mm × 20 mm sample with a 6 mm space in between. The sample was then fixed on a 75 μm thick Kapton polyimide support piece with double-sided tape, after which external

https://doi.org/10.1021/acsaelm.1c01175
ACS Appl. Electron. Mater. 2022, 4, 539−545

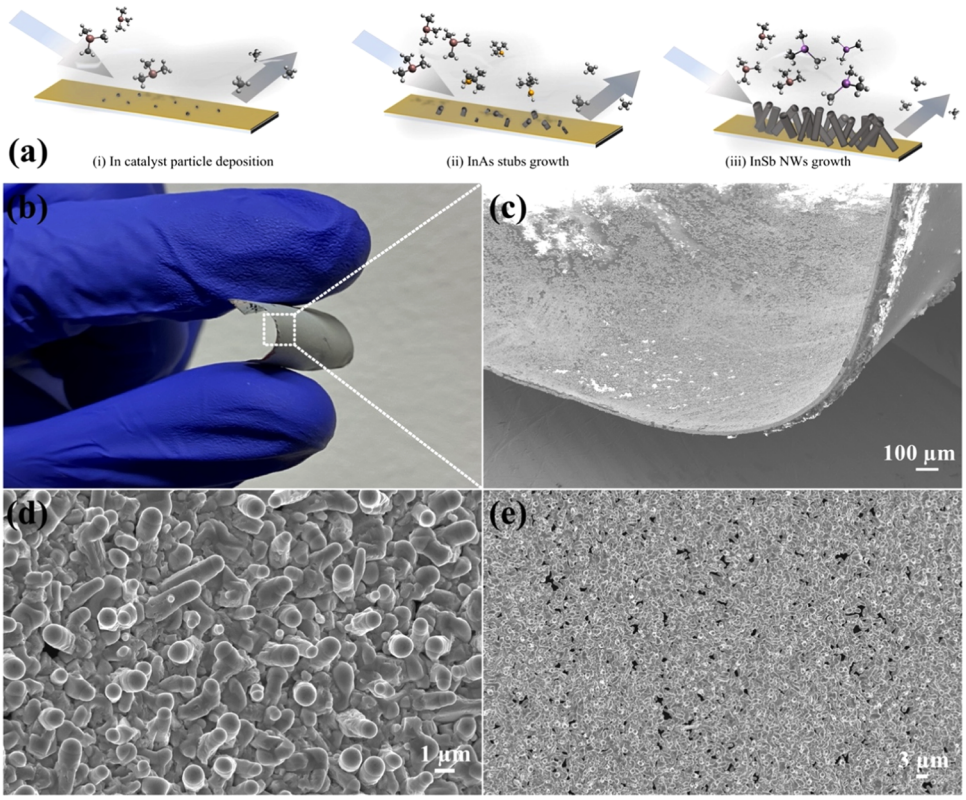

Figure 1. (a) Process schematic depicting the main steps in the growth process. (b) Photograph of the InSb NWs grown directly on flexible PI tape showing a high degree of flexibility. (c–e) SEM images of as-grown InSb NWs.

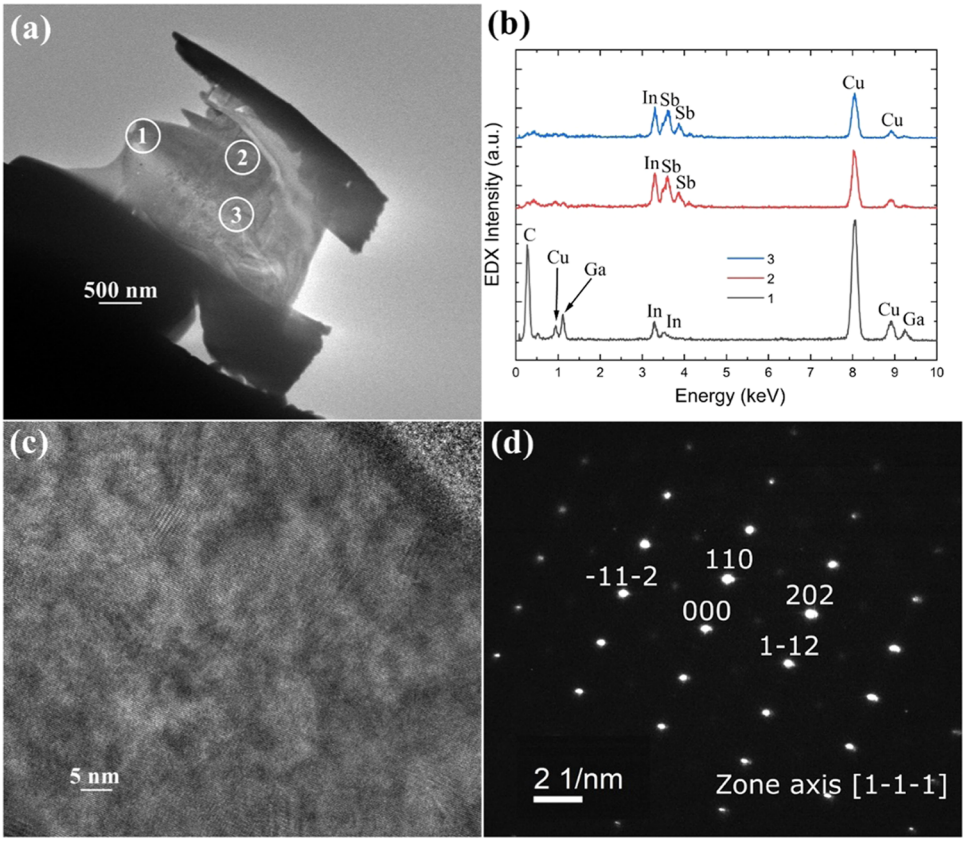

Figure 2. (a) Cross-sectional lamella of a typical InSb NW grown on PI. (b) EDX spectra corresponding to areas 1–3. (c) High-magnification image of area 2 and its (d) electron diffraction pattern corresponding to the ZB crystal structure.

https://doi.org/10.1021/acsaelm.1c01175
ACS Appl. Electron. Mater. 2022, 4, 539–545

wiring was fixed on the contact pads by silver epoxy (Polytec PU 1000). The bending measurement was conducted using a computer-controlled motorized stage. The bending radius was calculated at each stage position[33] while simultaneously recording the corresponding current−voltage characteristics (Keithley 2602B) to obtain the sample resistance. A complete bending cycle consisted of imposing tensile stress on the sample by moving the stage forward and then releasing the stress by bringing it back to the original position.

RESULTS AND DISCUSSION

InSb Nanowire Growth on Polyimide. InSb NWs were synthesized on flexible plastic substrates directly inside a horizontal-flow atmospheric-pressure metal−organic vapor-phase epitaxy. The three major steps in the growth process have been illustrated in a process schematic presented in Figure 1a. Briefly, In catalyst droplets were deposited in situ on the polyimide substrate, after which InAs stubs were grown under trimethylindium (TMIn) and tertiary butylarsine (TBAs) flows, followed by InSb crystal growth under TMI and trimethylantimony (TMSb) flows. Further details and detailed growth parameters are described in the Experimental Section. The image of InSb NWs grown directly on polyimide tape inside the MOVPE reactor is shown in Figure 1b bent in a hand. The originally bright yellow PI substrate turned gray due to the presence of NWs that trap light efficiently. Figure 1c−e shows a scanning electron microscopy (SEM) micrograph of InSb NWs. Similar to our previous work on InAs NWs,[23] the InSb NWs in this report tend to form a continuous interconnected network that covers the whole surface of the plastic substrate. To further clarify the structure, the InSb growth occurs simultaneously as out-of-plane NWs as well as growth on the plastic surface. This results in an interconnected network on the surface with NW forest on top. Both of these provide certain advantages; the network on the surface enables electrical contact between different points on the substrate, and NWs offer excellent light-trapping properties as will be discussed in more detail later in this paper.

TEM measurements were performed to investigate the crystal structure and chemical composition of the samples (Figure 2). Note that Figure 2a presents a lamella fabricated from the structure, i.e., a cross-sectional cut from the structure and not a single definite nanowire. The lamella was used as the InSb NWs in this study are relatively thick and therefore challenging to image directly with TEM. The TEM lamella was prepared as described in the Experimental Section. The low- and high-magnification TEM micrographs and the diffraction patterns confirm the crystalline nature of the NWs, and the diffraction pattern corresponds to zinc-blende (ZB) InSb (Figure 2d). In the diffraction pattern, the observed distances to the three closest diffraction spots were 0.455, 0.263, and 0.222 nm. In the InSb ZB crystal, these correspond closely to the crystal planes of 110 (0.458 nm), 211 (0.265 nm), and 220 (0.229 nm), respectively. Therefore, the observed crystal is determined to be ZB InSb, which is further evidenced by the PL peak position corresponding to ZB InSb as will be shown later in this paper.

Energy-dispersive X-ray spectroscopy (EDX) analysis further confirms that the crystal is pure InSb without additional detectable elements. Three different areas were measured from the lamella as marked in Figure 2a. In area "1", only In was observed, and thus this region corresponds to the In seed particle, indicating that the growth is seeded by a particle composed of indium. In regions "2" and "3", the presence of In and Sb was observed corresponding to NW body and/or network. Notably, no additional elements or impurities were detected since the C and Cu signals originate from the copper grid and stage used in the TEM measurements, while the Ga signal originates from the FIB processing that was used to prepare the lamella and thin it down. The absence of additional elements is an indication of the suitability of flexible polyimide substrates for crystal growth under the conditions used in this study.

Optical Properties of Nanowires on Polyimide. The possibility of growing high-quality InSb on polyimide substrates is further highlighted by photoluminescence properties. Figure 3 shows the typical PL spectra measured from the as-grown, unpassivated InSb NWs directly on polyimide. A strong and clear PL peak is observed even at room temperature, further suggesting the high optical quality of the crystal. The dominant peak is observed at ∼155 meV, which is close to the ZB InSb band gap energy and is in agreement with previous studies, where the band gap was estimated from absorption measurements.[34,35] Importantly, here, we report for the first time directly measured photoluminescence from InSb nanowires. The observed PL peak of ∼155 meV is slightly red-shifted by ∼15 meV from the ZB InSb band gap value. On the other hand, red-shifting of PL signal in nanowires is a common phenomenon with various origins: (i) band bending related to surface states[36] or interfaces;[37] (ii) crystal structure variation, type II transitions, and defects;[38,39] and (iii) dopants and impurities.[39,40] Here, red-shifting due to surface and interface states is considered the most plausible explanation since the InSb network on the PI surface is of polycrystalline nature and is expected to contain grain boundaries, and additionally, the InSb NW structure has a high surface-to-volume ratio. Similarly, impurities may be present in the NWs in quantities below the EDX detection limit and induce red-shifting of the PL peak position. Red-shifting due to crystal structure variation is considered less likely as only the ZB phase was observed in TEM. Finally, it should be noted here that the redshift of the PL signal may be in fact beneficial for photodetection purposes, as it can extend the detectable wavelength range.

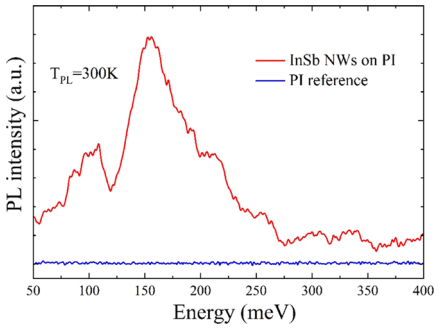

Figure 3. Photoluminescence spectrum of InSb NWs on the flexible plastic substrate at RT.

Another attractive property of the InSb nanowire network is low reflectance, as depicted in Figure 4 (reflectance spectrum is shown from InSb NWs on PI). The NW samples have a very low reflectance of 5−9% in the whole relevant mid- and long-wave infrared range (compared to 30−40% of the bulk in the same range[41,42]), which confirms their outstanding light-trapping properties. In fact, originally bright yellow and

https://doi.org/10.1021/acsaelm.1c01175
ACS Appl. Electron. Mater. 2022, 4, 539−545

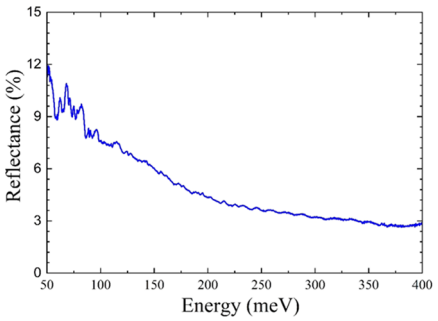

Figure 4. Reflectance spectrum from InSb NWs on PI.

moderately reflective and transparent PI tape turns dark gray after the NW synthesis. The naturally low reflectance of the NWs presented here is advantageous compared to planar epitaxial or amorphous films, as it omits the need for externally fabricated antireflection coatings and allows their straightforward application to photodetection. This is particularly important for InSb, as one of its primary application areas is photodetection. Furthermore, NWs and plastics are flexible, which makes InSb NWs on plastic particularly promising for nanowire-based flexible IR and broad-band high absorption optoelectronic applications where low reflectance and high absorptance are crucial.

Electrical Properties and Photoresistor Demonstration. The final device structure (depicted in Figure 5a) was finalized by evaporating Ti/Au (20/100 nm) rectangle contact pads (4 mm × 7 mm) through a shadow mask at the ends of the sample with a separation of 6 mm in between. Hence, the photoresistor was fabricated monolithically on a flexible substrate in only two steps: InSb NW growth in MOVPE, followed by Ti/Au contact pads evaporation. Figure 5b presents the current−voltage characteristics of the InSb sample in the dark and under illumination (AM1.5). Both curves show a linear trend implying ohmic behavior. When the sample is illuminated, we observe a positive shift in the slope of the curve caused by the photoexcited charge carriers. This shows that the InSb NWs grown on plastic are not only of high optical quality but also applicable to device structures. Figure 5c further shows the effect of illumination on the sample resistance when the light source is chopped on and off at a 2 s interval. Compared to its state in the dark, the sample resistance shows a ∼5% average decrease when under illumination. Here, we aim to demonstrate that the InSb NWs on plastic are applicable to photoconductive devices, whereas in future work, we expect the InSb material to be applied for more detailed and specialized applications, such as IR photodetection and more sophisticated device structures, such as nbn-type detectors.[43] It should be further noted that the demonstrated photoresistor fabrication process required just two processing steps: (1) InSb growth on plastic without any substrate preparation steps and (2) metal contact deposition.

The mechanical flexibility of the InSb nanowire film was investigated by controlled bending of the sample to induce tensile stress on the film. The relative change in resistance as a function of bending radius during a single bending cycle is presented in Figure 6a. The sample shows a critical bending radius at ∼8 mm, after which the resistance increases by 1.5% without returning to the initial value when the sample is unbent. The result implies that the film should withstand bending to radii larger than 8 mm, thus enabling practical

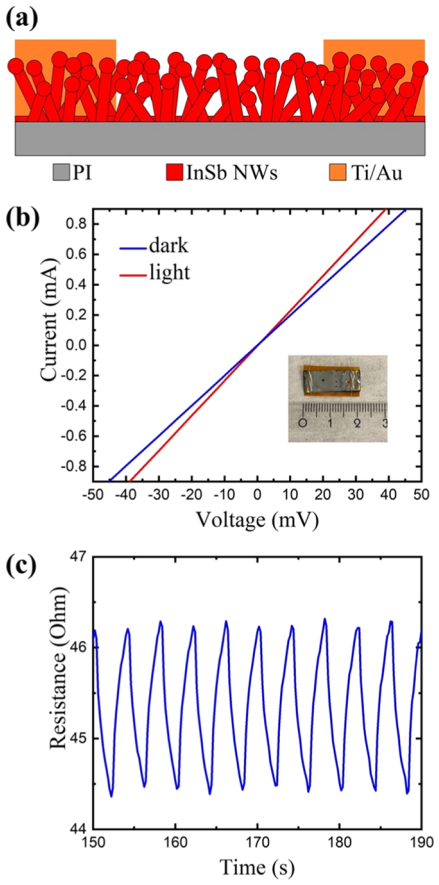

Figure 5. (a) Schematic structure of the device. (b) Current−voltage characteristics of InSb NWs on PI in the dark (blue) and under illumination (red) (AM1.5); the inset depicts a photograph of the device. (c) Change in resistance InSb NWs on PI in the dark and under illumination as a function of time.

devices that can be attached on various curved surfaces. Further evidence of practical device applicability is gained by tensile bending of a second sample to a bending radius of 15 mm multiple times as presented in Figure 6b. The sample withstands consecutive bending extremely well with under 10% relative change in resistance after 1500 bending cycles, implying suitability to practical device use. In addition, by optimizing the InSb NW network in future work, we expect that an even higher degree of flexibility can be attained.

CONCLUSIONS

We have demonstrated for the first time the growth of InSb nanowires by MOVPE directly on flexible plastic substrates. We have shown that the nanowires crystallize in the ZB structure, and importantly, the material quality allowed the first measurement of InSb NW photoluminescence at room temperature. The PL characterization revealed a band gap of ∼170 meV, which corresponds to earlier values of the ZB InSb band gap. As is typically observed for surfaces covered by NWs, the reflectance of the InSb network was found to be very low in the relevant IR wavelength range. The InSb nanowires were further shown to be applicable to optoelectronic devices by fabricating a photoresistor structure. Finally, the structures were shown to withstand bending to a relatively small radius. We believe this will advance the development of nanowire-based flexible optoelectronics and simultaneously enable

https://doi.org/10.1021/acsaelm.1c01175
ACS Appl. Electron. Mater. 2022, 4, 539−545

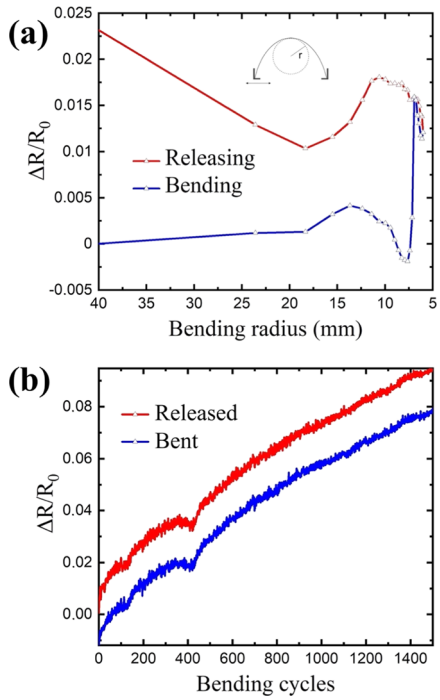

Figure 6. (a) Relative change in resistance under tensile stress as a function of bending radius. (b) Relative change in resistance as a function of bending cycles.

straightforward fabrication of infrared photodetectors and other relevant devices.

AUTHOR INFORMATION

Corresponding Author

Vladislav Khayrudinov − *Department of Electronics and Nanoengineering, Micronova, Aalto University, FI-00076 Espoo, Finland;* orcid.org/0000-0002-4125-6104; Email: vladislav.khayrudinov@aalto.fi

Authors

Tomi Koskinen − *Department of Electronics and Nanoengineering, Micronova, Aalto University, FI-00076 Espoo, Finland;* orcid.org/0000-0001-6883-4181

Kacper Grodecki − *Institute of Applied Physics, Military University of Technology, 00-908 Warsaw, Poland*

Krzysztof Murawski − *Institute of Applied Physics, Military University of Technology, 00-908 Warsaw, Poland*

Małgorzata Kopytko − *Institute of Applied Physics, Military University of Technology, 00-908 Warsaw, Poland*

Lide Yao − *Department of Applied Physics, Aalto University, FI-00076 Espoo, Finland*

Hua Jiang − *Department of Applied Physics, Aalto University, FI-00076 Espoo, Finland*

Ilkka Juhani Tittonen − *Department of Electronics and Nanoengineering, Micronova, Aalto University, FI-00076 Espoo, Finland;* orcid.org/0000-0002-2985-9789

Harri Lipsanen − *Department of Electronics and Nanoengineering, Micronova, Aalto University, FI-00076 Espoo, Finland;* orcid.org/0000-0003-2487-4645

Tuomas Haggren − *Department of Electronics and Nanoengineering, Micronova, Aalto University, FI-00076 Espoo, Finland;* orcid.org/0000-0001-6033-7391

Complete contact information is available at: https://pubs.acs.org/10.1021/acsaelm.1c01175

Notes

The authors declare no competing financial interest.

ACKNOWLEDGMENTS

V.K. acknowledges the support of Aalto University Doctoral School, Walter Ahlström Foundation, Elektroniikkainsinöörien Säätiö, Sähköinsinööriliiton Säätiö, Nokia Foundation, Finnish Foundation for Technology Promotion (Tekniikan Edistämissäätiö), Waldemar von Frenckell's Foundation, and Kansallis-Osake-Pankki fund. T.K. acknowledges the support of Aalto University Doctoral School and Walter Ahlström Foundation. T.H. acknowledges the support of the Finnish Cultural Foundation and Walter Ahlström Foundation. The Academy of Finland Photonics Flagship PREIN is acknowledged. The authors thank Lassi Hällström for the help with the solar simulator measurements. The authors acknowledge the provision of facilities and technical support by Aalto University at Micronova Nanofabrication Centre and Nanomicroscopy Center.

REFERENCES

(1) Li, C.; Liu, Z.; Chen, J.; Gao, Y.; Li, M.; Zhang, Q. Semiconductor Nanowire Plasmonic Lasers. *Nanophotonics* **2019**, *8*, 2091−2110.

(2) Huang, M. H.; Mao, S.; Feick, H.; Yan, H.; Wu, Y.; Kind, H.; Weber, E.; Russo, R.; Yang, P. Room-Temperature Ultraviolet Nanowire Nanolasers. *Science* **2001**, *292*, 1897−1899.

(3) Eaton, S. W.; Fu, A.; Wong, A. B.; Ning, C. Z.; Yang, P. Semiconductor Nanowire Lasers. *Nat. Rev. Mater.* **2016**, *1*, No. 16028.

(4) Qian, F.; Gradečak, S.; Li, Y.; Wen, C.-Y.; Lieber, C. M. Core/Multishell Nanowire Heterostructures as Multicolor, High-Efficiency Light-Emitting Diodes. *Nano Lett.* **2005**, *5*, 2287−2291.

(5) Yang, H.; Khayrudinov, V.; Dhaka, V.; Jiang, H.; Autere, A.; Lipsanen, H.; Sun, Z.; Jussila, H. Nanowire Network−Based Multifunctional All-Optical Logic Gates. *Sci. Adv.* **2018**, *4*, No. eaar7954.

(6) Wallentin, J.; Anttu, N.; Asoli, D.; Huffman, M.; Åberg, I.; Magnusson, M. H.; Siefer, G.; Fuss-Kailuweit, P.; Dimroth, F.; Witzigmann, B.; Xu, H. Q.; et al. InP Nanowire Array Solar Cells Achieving 13. 8% Efficiency by Exceeding the Ray Optics Limit. *Science* **2013**, *339*, 1057−1060.

(7) Miao, J.; Hu, W.; Guo, N.; Lu, Z.; Zou, X.; Liao, L.; Shi, S.; Chen, P.; Fan, Z.; Ho, J. C.; Li, T. X.; et al. Single InAs Nanowire Room-Temperature Near-Infrared Photodetectors. *ACS Nano* **2014**, *8*, 3628−3635.

(8) Hu, P.; Wang, L.; Yoon, M.; Zhang, J.; Feng, W.; Wang, X.; Wen, Z.; Idrobo, J. C.; Miyamoto, Y.; Geohegan, D. B.; Xiao, K. Highly Responsive Ultrathin GaS Nanosheet Photodetectors on Rigid and Flexible Substrates. *Nano Lett.* **2013**, *13*, 1649−1654.

(9) Chen, Y.; Li, H.; Li, M. Flexible and Tunable Silicon Photonic Circuits on Plastic Substrates. *Sci. Rep.* **2012**, *2*, No. 622.

(10) Koo, M.; Park, K.-I.; Lee, S. H.; Suh, M.; Jeon, D. Y.; Choi, J. W.; Kang, K.; Lee, K. J. Bendable Inorganic Thin-Film Battery for Fully Flexible Electronic Systems. *Nano Lett.* **2012**, *12*, 4810−4816.

(11) Han, N.; Yang, Z.; Wang, F.; Dong, G.; Yip, S.; Liang, X.; Hung, T. F.; Chen, Y.; Ho, J. C. High-Performance GaAs Nanowire Solar Cells for Flexible and Transparent Photovoltaics. *ACS Appl. Mater. Interfaces* **2015**, *7*, 20454−20459.

(12) Kenry; Yeo, J. C.; Lim, C. T. Emerging Flexible and Wearable Physical Sensing Platforms for Healthcare and Biomedical Applications. *Microsyst. Nanoeng.* **2016**, *26*, No. 16043.

(13) Haggren, T.; Anttu, N.; Mäntynen, H.; Tossi, C.; Kim, M.; Khayrudinov, V.; Lipsanen, H. Management of Light and Scattering in InP NWs by Dielectric Polymer Shell. *Nanotechnology* **2020**, *31*, No. 384003.

(14) Joyce, H. J.; Gao, Q.; Tan, H. H.; Jagadish, C.; Kim, Y.; Zou, J.; Smith, L. M.; Jackson, H. E.; Yarrison-Rice, J. M.; Parkinson, P.;

Johnston, M. B. III − V Semiconductor Nanowires for Optoelectronic Device Applications. *Prog. Quantum Electron.* **2011**, *35*, 23−75.
(15) Kuo, C. H.; Wu, J. M.; Lin, S. J.; Chang, W. C. High Sensitivity of Middle-Wavelength Infrared Photodetectors Based on an Individual InSb Nanowire. *Nanoscale Res. Lett.* **2013**, *8*, No. 327.
(16) Nilsson, H. A.; Deng, M. T.; Caroff, P.; Thelander, C.; Samuelson, L.; Wernersson, L. E.; Xu, H. Q. InSb Nanowire Field-Effect Transistors and Quantum-Dot Devices. *IEEE J. Sel. Top. Quantum Electron.* **2011**, *17*, 907−914.
(17) Nilsson, H. A.; Samuelsson, P.; Caroff, P.; Xu, H. Q. Supercurrent and Multiple Andreev Reflections in an InSb Nanowire Josephson Junction. *Nano Lett.* **2012**, *12*, 228−233.
(18) Yip, S.; Shen, L.; Ho, J. C. Recent Advances in III-Sb Nanowires: From Synthesis to Applications. *Nanotechnology* **2019**, *30*, No. 202003.
(19) Valente, J.; Godde, T.; Zhang, Y.; Mowbray, D. J.; Liu, H. Light-Emitting GaAs Nanowires on a Flexible Substrate. *Nano Lett.* **2018**, *18*, 4206−4213.
(20) Liu, X.; Long, Y.-Z.; Liao, L.; Duan, X.; Fan, Z. Large-Scale Integration of Semiconductor Nanowires for High-Performance Flexible Electronics. *ACS Nano* **2012**, *6*, 1888−1900.
(21) McAlpine, M. C.; Ahmad, H.; Wang, D.; Heath, J. R. Highly Ordered Nanowire Arrays on Plastic Substrates for Ultrasensitive Flexible Chemical Sensors. *Nat. Mater.* **2007**, *6*, 379−384.
(22) Cavalli, A.; Dijkstra, A.; Haverkort, J. E. M.; Bakkers, E. P. A. M. Nanowire Polymer Transfer for Enhanced Solar Cell Performance and Lower Cost. *Nano-Struct. Nano-Objects* **2018**, *16*, 59−62.
(23) Khayrudinov, V.; Remennyi, M.; Raj, V.; Alekseev, P.; Matveev, B.; Lipsanen, H.; Haggren, T. Direct Growth of Light-Emitting III−V Nanowires on Flexible Plastic Substrates. *ACS Nano* **2020**, *14*, 7484−7491.
(24) Haggren, T.; Khayrudinov, V.; Dhaka, V.; Jiang, H.; Shah, A.; Kim, M.; Lipsanen, H. III−V Nanowires on Black Silicon and Low-Temperature Growth of Self-Catalyzed Rectangular InAs NWs. *Sci. Rep.* **2018**, *8*, No. 6410.
(25) Caroff, P.; Messing, M. E.; Borg, B. M.; Dick, K. A.; Deppert, K.; Wernersson, L.-E. InSb Heterostructure Nanowires: MOVPE Growth under Extreme Lattice Mismatch. *Nanotechnology* **2009**, *20*, No. 495606.
(26) Anandan, D.; Nagarajan, V.; Kakkerla, R. K.; Yu, H. W.; Ko, H. L.; Singh, S. K.; Lee, C. T.; Chang, E. Y. Crystal Phase Control in Self-Catalyzed InSb Nanowires Using Basic Growth Parameter V/III Ratio. *J. Cryst. Growth* **2019**, *522*, 30−36.
(27) Jin, Y. J.; Zheng, X. E.; Gong, S. J.; Ke, C.; Xiao, M. Q.; Ling, B.; Yu, S. Y.; Zhang, D. H. Hetero-Epitaxial Growth and Mechanism of One-Dimensional InSb Nanostructures on GaAs Substrate by MOCVD. *J. Alloys Compd.* **2020**, *823*, No. 153758.
(28) Jin, Y. J.; Zhang, D. H.; Liu, H. F.; Tang, X. H. Self-Nucleation Growth of InSb Nanowires Based on Indium Droplets under the Assistance of Au Nano-Particles by MOCVD. *Mater. Lett.* **2016**, *185*, 77−80.
(29) Jin, Y. J.; Tang, X. H.; Liu, H. F.; Ke, C.; Wang, S. J.; Zhang, D. H. Growth of One-Dimensional InSb Nanostructures with Controlled Orientations on InSb Substrates by MOCVD. *J. Alloys Compd.* **2017**, *721*, 628−632.
(30) Badawy, G.; Gazibegovic, S.; Borsoi, F.; Heedt, S.; Wang, C. A.; Koelling, S.; Verheijen, M. A.; Kouwenhoven, L. P.; Bakkers, E. P. A. M. High Mobility Stemless InSb Nanowires. *Nano Lett.* **2019**, *19*, 3575−3582.
(31) Singh, A. P.; Roccapriore, K.; Algarni, Z.; Salloom, R.; Golden, T. D.; Philipose, U. Structure and Electronic Properties of InSb Nanowires Grown in Flexible Polycarbonate Membranes. *Nanomaterials* **2019**, *9*, No. 1260.
(32) Dick, K. A. A Review of Nanowire Growth Promoted by Alloys and Non-Alloying Elements with Emphasis on Au-Assisted III e V Nanowires. *Prog. Cryst. Growth Charact. Mater.* **2008**, *54*, 138−173.
(33) Park, S. Il.; Ahn, J. H.; Feng, X.; Wang, S.; Huang, Y.; Rogers, J. A. Theoretical and Experimental Studies of Bending of Inorganic Electronic Materials on Plastic Substrates. *Adv. Funct. Mater.* **2008**, *18*, 2673−2684.
(34) Algarni, Z.; George, D.; Singh, A.; Lin, Y.; Philipose, U. Hole-Dominated Transport in InSb Nanowires Grown on High-Quality InSb Films. *J. Nanopart. Res.* **2016**, *18*, No. 361.
(35) Yang, Y.; Li, L.; Huang, X.; Li, G.; Zhang, L. Fabrication and Optical Property of Single-Crystalline InSb Nanowire Arrays. *J. Mater. Sci.* **2007**, *42*, 2753−2757.
(36) Van Weert, M. H. M.; Wunnicke, O.; Roest, A. L.; Eijkemans, T. J.; Silov, A. Y.; Haverkort, J. E. M.; 'T Hooft, G. W.; Bakkers, E. P. A. M. Large Redshift in Photoluminescence of P-Doped InP Nanowires Induced by Fermi-Level Pinning. *Appl. Phys. Lett.* **2006**, *88*, No. 043109.
(37) Dhaka, V.; Oksanen, J.; Jiang, H.; Haggren, T.; Nykänen, A.; Sanatinia, R.; Kakko, J. P.; Huhtio, T.; Mattila, M.; Ruokolainen, J.; Anand, S.; et al. Aluminum-Induced Photoluminescence Red Shifts in Core-Shell GaAs/Al XGa1-XAs Nanowires. *Nano Lett.* **2013**, *13*, 3581−3588.
(38) Spirkoska, D.; Arbiol, J.; Gustafsson, A.; Conesa-Boj, S.; Glas, F.; Zardo, I.; Heigoldt, M.; Gass, M. H.; Bleloch, A. L.; Estrade, S.; Kaniber, M.; et al. Structural and Optical Properties of High Quality Zinc-Blende/Wurtzite GaAs Nanowire Heterostructures. *Phys. Rev. B* **2009**, *80*, No. 245325.
(39) Haggren, T.; Otnes, G.; Mourão, R.; Dagyte, V.; Hultin, O.; Lindelöw, F.; Borgström, M.; Samuelson, L. InP Nanowire P-Type Doping via Zinc Indiffusion. *J. Cryst. Growth* **2016**, *451*, 18−26.
(40) Haggren, T.; Perros, A.; Dhaka, V.; Huhtio, T.; Jussila, H.; Jiang, H.; Ruoho, M.; Kakko, J. P.; Kauppinen, E.; Lipsanen, H. GaAs Nanowires Grown on Al-Doped ZnO Buffer Layer. *J. Appl. Phys.* **2013**, *114*, No. 084309.
(41) McCarthy, D. E. The Reflection and Transmission of Infrared Materials V: Spectra from 2 μ to 50 μ. *Appl. Opt.* **1968**, *7*, No. 1997.
(42) Bate, G.; Taylor, K. N. R. Production and Properties of Thin Layers of Indium Antimonide. *J. Appl. Phys.* **1960**, *31*, 991−994.
(43) Evirgen, A.; Abautret, J.; Perez, J. P.; Cordat, A.; Nedelcu, A.; Christol, P. Midwave Infrared InSb NBn Photodetector. *Electron. Lett.* **2014**, *50*, 1472−1473.

https://doi.org/10.1021/acsaelm.1c01175
ACS Appl. Electron. Mater. 2022, 4, 539−545